Computer Assisted Mechanics and Engineering Sciences, 6: 369–383, 1999.

FE analysis of geometrically nonlinear static problems with follower loads

Imre Kozák, Frigges Nándori
Department of Mechanics, University of Miskolc

Tamás Szabó
Hungarian Academy of Sciences – University of Miskolc,
Numerical Mechanics Research Group

(Received March 8, 1999)

We have considered a linearly elastic body loaded by tractions inward normal to the instantaneous surface. Due to the increment of the surface element vector there is a contribution to the tangent stiffness matrix referred to as load correction stiffness matrix. The goal of the numerical experiments is to determine the bifurcation point on the fundamental equilibrium path. Linear eigenvalue problems with follower loads are also analysed.

Keywords: follower loads, finite element method, limit of elastic stability, eigenvalue problem

1. Introduction

A typical problem of continuum mechanics is the determination of critical loads of conservative and non-conservative mechanical systems. For non-conservative systems this is performed usually by dynamical methods.

A number of excellent monographs are devoted to the investigation of the stability behavior of conservative systems, e.g., Thompson and Hunt [20, 21], Huseyin [11], Thompson [19], Guz [9] and Crisfield [7]. Relatively few monographs are concerned with the stability of non-conservative systems, e.g., Bolotin [5]. For a normal pressure field with potential Koiter [12] derived the so-called "pressure stiffness matrix" referred to as load correction stiffness matrix in the present paper. Conservativeness of a normal pressure field has been studied by Cohen [6] and Hibbitt [10]. Loganathan, Chang, Gallagher and Abel [14] have reviewed analytical as well as numerical works on the effects of follower forces in stability analysis. Mang [15] raised the issue of making the originally non-symmetric pressure stiffness matrix to be symmetric. Then Floegel and Mang [8] performed finite element computations by the use of symmetrized pressure stiffness matrices. The above citations should be supplemented by the excellent dissertation of Schweizerhof [16]. Further contributions with various approaches are published in the papers by Argyiris and Symeonidis [3, 4], Argyiris, Straub and Symeonidis [1, 2]. The references listed in them provide a further insight to the background of the problem.

The present paper is concerned with the investigation of elastic systems with follower loads using static methods for some three-dimensional and geometrically nonlinear models.

In Section 2 we formulate the change of the vectorial surface element as a function of the deformations. The principle of virtual displacement in incremental formulation and its linearized form are also given with a special attention to the increment of the surface element vector. Our approach to finding the nonlinear response of the body is an incremental iterative method. It is advantageous to take into consideration the increment of the surface element vector in the incremental formula too,

as our numerical experiments confirmed that the number of equilibrium iterations was decreased significantly in this way.

In Section 3 the critical load is determined with a path following method for a circular ring loaded by a uniform normal load $\tilde{p}$. The critical value of $\tilde{p}$ is understood to be the smallest value of $\tilde{p}$ at which bifurcation occurs on the fundamental equilibrium path. Equilibrium paths are also determined for rings with geometrical imperfections, that is, the circular ring is replaced by an elliptical ring. In the first case the minor axis of the centre line is smaller by 0.5% than the major axis. In the second case the value is 0.05%. However, the major axis is equal to the mean radius of the circular ring for both cases.

Section 4 is devoted to linear eigenvalue problems with an emphasis on the role of the increment of the surface element vector in three-dimensional problems.

2. Formulation of the problem

2.1. Configurations and change of the vectorial surface element

According to Fig. 1, we distinguish the stress and deformation free reference configuration, which is denoted by (B), from the following two types of configurations. The first type is the present or instantaneous configuration denoted by $(\bar{B})$, which is in equilibrium under the given loads. By the second type we mean the intermediate configurations denoted by $(B'_{\underline{s}})$, where the underlined subscripts $\underline{s} = \underline{1}, \underline{2}, \ldots, \underline{n}$ indicates the iteration number. When the subscript $\underline{s}$ is equal to $\underline{1}$, the configuration $(B'_{\underline{1}})$ is called initial configuration.

Applying the total Lagrangian description the following notations are used in the reference configuration (B): $\mathrm{d}\mathbf{A}$ is the surface element vector, $\mathbf{u}, \boldsymbol{E}, \boldsymbol{S}$ are the displacement vector, the Green–Lagrange strain tensor, the 2nd Piola–Kirchhoff stress tensor and $\Delta\mathbf{u}$, $\Delta\boldsymbol{E}$, $\Delta\boldsymbol{S}$ are their increments, respectively. The virtual displacement vector is $\delta\boldsymbol{u} = \delta(\Delta\boldsymbol{u})$.

The 2nd Piola–Kirchhoff stress tensor is related to the Green–Lagrange strain tensor by Hooke's law:

$$\boldsymbol{S} = {}^{[4]}\boldsymbol{C} \cdot\cdot \boldsymbol{E} = \boldsymbol{E} \cdot\cdot {}^{[4]}\boldsymbol{C} \tag{1}$$

where ${}^{[4]}\mathbf{C}$ is the forth order tensor of material properties.

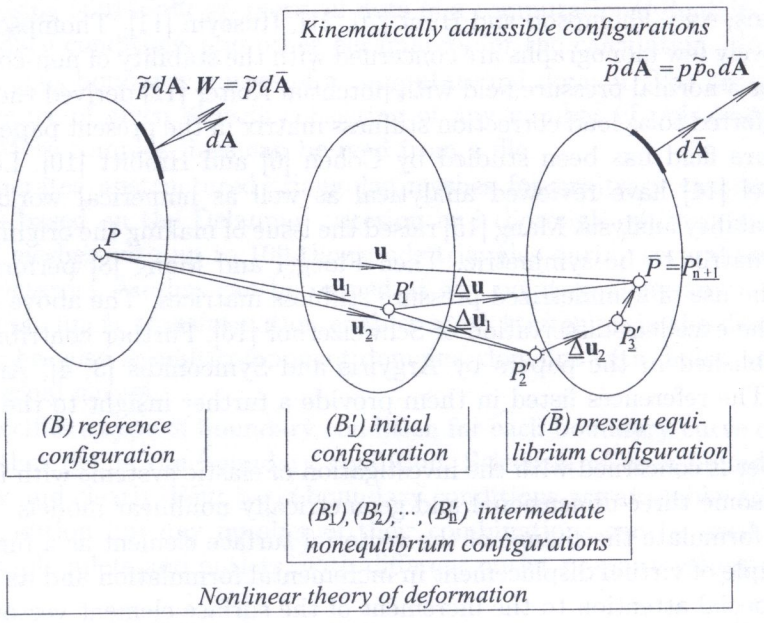

Fig. 1. Configurations

In the present configuration $(\bar{B})$ the surface element vector is denoted by $d\bar{\mathbf{A}}$. The body forces are disregarded in our investigation. By $\tilde{p}$ we denote the normal traction acting on the surface $(\bar{A}_t)$. Then the force vector $d\mathbf{F}$ acting on an surface element $d\bar{\mathbf{A}}$ is

$$d\mathbf{F} = \tilde{p}\, \mathrm{d}\bar{\mathbf{A}}, \qquad \tilde{p} = p\tilde{p}_\circ, \tag{2}$$

where $p > 0$ is a load factor, $\tilde{p}_\circ$ is a normal load distribution which is positive if it points out of (B).

The relation between the surface element vectors of the two configurations is given by

$$\mathrm{d}\bar{\mathbf{A}} = \mathrm{d}\mathbf{A} \cdot \boldsymbol{W} \tag{3}$$

where

$$W^l_{\ p} = \frac{1}{2} e^{lmn} e_{pqr} \left(\delta^q_{\ m} + u^q{}_{;m}\right) \left(\delta^r_{\ n} + u^r{}_{;n}\right), \tag{4}$$

in which e^{lmn}, e_{pqr} are the perturbation symbols, δ^q_m, δ^r_n are the unit tensors and the subscripts preceded by a semicolon denote covariant derivatives with respect to the corresponding coordinate.

With regard to (3) the increment of the surface element vector $\Delta\left(\mathrm{d}\bar{\mathbf{A}}\right)$ can be expressed as

$$\Delta\left(\mathrm{d}\bar{\mathbf{A}}\right) = \mathrm{d}\mathbf{A} \cdot \Delta\boldsymbol{W}. \tag{5}$$

The increment $\Delta\boldsymbol{W}$ can be decomposed into linear and quadratic terms which are denoted by $\Delta\boldsymbol{W}^{(1)}$ and $\Delta\boldsymbol{W}^{(2)}$ respectively

$$\Delta\boldsymbol{W} = \Delta\boldsymbol{W}^{(1)} + \Delta\boldsymbol{W}^{(2)}, \tag{6}$$

where

$$\left(\Delta W^{(1)}\right)^l_{\ p} = e^{lmn} e_{pqr} \left(\delta^q_{\ m} + u^q{}_{;m}\right) (\Delta u)^r{}_{;n}, \tag{7}$$

$$\left(\Delta W^{(2)}\right)^l_{\ p} = \frac{1}{2} e^{lmn} e_{pqr} \, (\Delta u)^q{}_{;m} \, (\Delta u)^r{}_{;n}. \tag{8}$$

Here and in the sequel the number written as a superscript in parentheses is the power of the components of $(\Delta\mathbf{u})\nabla$.

Using (7) we may write

$$\mathrm{d}A_l \left(\Delta W^{(1)}\right)^l_{\ p} = e_{pqr} \left[\mathrm{d}A_l \, e^{lmn} \left(\delta^q_{\ m} + u^q{}_{;m}\right) (\Delta u)^r{}_{;n}\right] = D_{pr} \, (\Delta u)^r \tag{9}$$

where D_{pr} is a special differential operator.

2.2. Incremental form of the principle of virtual displacements

Let the vector $\mathbf{u}_{\underline{1}}$ be an appropriately chosen otherwise arbitrary kinematically admissible displacement field associated with the initial configuration $(B'_{\underline{1}})$. The configuration $(B'_{\underline{1}})$ is not an equilibrium configuration of the load $\tilde{p}$. This assumption does not precludes the possibility that $(B'_{\underline{1}})$ is an initial equilibrium configuration under a load $\tilde{p}_{\underline{1}} \neq \tilde{p}$.

In the present equilibrium configuration $(\bar{B})$, which is due to the load $\tilde{p}$, we write (δ denotes a virtual quantity)

$$\mathbf{u} = \mathbf{u}_{\underline{1}} + \Delta\mathbf{u}_{\underline{1}}, \qquad \delta\mathbf{u} = \delta\left(\Delta\mathbf{u}_{\underline{1}}\right), \tag{10}$$

$$\boldsymbol{E} = \boldsymbol{E}_{\underline{1}} + \Delta\boldsymbol{E}_{\underline{1}} = \boldsymbol{E}_{\underline{1}} + \Delta\boldsymbol{E}^{(1)}_{\underline{1}} + \Delta\boldsymbol{E}^{(2)}_{\underline{1}}, \tag{11}$$

$$\delta\boldsymbol{E} = \delta\left(\Delta\boldsymbol{E}_{\underline{1}}\right) = \delta\left(\Delta\boldsymbol{E}^{(1)}_{\underline{1}}\right) + \delta\left(\Delta\boldsymbol{E}^{(2)}_{\underline{1}}\right) = \delta\boldsymbol{E}^{(0)}_{\underline{1}} + \delta\boldsymbol{E}^{(1)}_{\underline{1}}, \tag{12}$$

$$\boldsymbol{S} = \boldsymbol{S}_{\underline{1}} + \Delta\boldsymbol{S}_{\underline{1}} = \boldsymbol{S}_{\underline{1}} + \Delta\boldsymbol{S}^{(1)}_{\underline{1}} + \Delta\boldsymbol{S}^{(2)}_{\underline{1}} \tag{13}$$

where

$$\boldsymbol{S}_{\underline{1}} = \boldsymbol{E} \cdot\cdot^{[4]} \boldsymbol{E}, \qquad \Delta \boldsymbol{S}_{\underline{1}}^{(1)} = \Delta \boldsymbol{E}_{\underline{1}}^{(1)} \cdot\cdot^{[4]} \boldsymbol{C}, \qquad \Delta \boldsymbol{S}_{\underline{1}}^{(2)} = \Delta \boldsymbol{E}_{\underline{1}}^{(2)} \cdot\cdot^{[4]} \boldsymbol{E}. \tag{14}$$

According to the equations (3)–(8) the surface element vector is of the form

$$\mathrm{d}\bar{\mathbf{A}} = \mathrm{d}\bar{\mathbf{A}}_{\underline{1}} + \Delta\left(\mathrm{d}\bar{\mathbf{A}}_{\underline{1}}\right) = \mathrm{d}\mathbf{A} \cdot \boldsymbol{W}_{\underline{1}} + \mathrm{d}\mathbf{A} \cdot \Delta \boldsymbol{W}_{\underline{1}}^{(1)} + \mathrm{d}\mathbf{A} \cdot \Delta \boldsymbol{W}_{\underline{1}}^{(2)}. \tag{15}$$

Formulas (11), (12) and (14) are detailed in the Appendix.

The present configuration $\left(\bar{B}\right)$ with the load $\tilde{p} = p\,\tilde{p}_{\mathrm{o}}$ is regarded as an equilibrium configuration if the principle of virtual displacements holds for arbitrary $\delta\mathbf{u}$:

$$\int_{(B)} \boldsymbol{S} \cdot\cdot\, \delta \boldsymbol{E}\, \mathrm{d}V = p \int_{(\bar{A}_t)} \tilde{p}_{\mathrm{o}}\, \mathrm{d}\bar{\mathbf{A}} \cdot \delta\mathbf{u}, \tag{16a}$$

from which using (10)-(15) we have

$$\int_{(B)} \left(\boldsymbol{S}_{\underline{1}} + \Delta \boldsymbol{S}_{\underline{1}}^{(1)} + \Delta \boldsymbol{S}_{\underline{1}}^{(2)}\right) \cdot\cdot \left(\delta \boldsymbol{E}_{\underline{1}}^{(0)} + \delta \boldsymbol{E}_{\underline{1}}^{(1)}\right) \mathrm{d}V \tag{16b}$$

$$= p \int_{(\bar{A}_t)} \tilde{p}_{\mathrm{o}}\, \mathrm{d}\mathbf{A} \cdot \left(\boldsymbol{W}_{\underline{1}} + \Delta \boldsymbol{W}_{\underline{1}}^{(1)} + \Delta \boldsymbol{W}_{\underline{1}}^{(2)}\right) \cdot \delta\mathbf{u}, \tag{16c}$$

Rewriting (16c) we obtain the incremental form of the principle of virtual displacement

$$\begin{aligned} &\int_{(B)} \left(\Delta \boldsymbol{S}_{\underline{1}}^{(1)} \cdot\cdot\, \delta \boldsymbol{E}_{\underline{1}}^{(0)} + \boldsymbol{S}_{\underline{1}} \cdot\cdot\, \delta \boldsymbol{E}_{\underline{1}}^{(1)}\right) \mathrm{d}V - p \int_{(\bar{A}_t)} \tilde{p}_{\mathrm{o}}\, \mathrm{d}\mathbf{A} \cdot \Delta \boldsymbol{W}_{\underline{1}}^{(1)} \cdot \delta\mathbf{u} \\ &- p \int_{(\bar{A}_t)} \tilde{p}_{\mathrm{o}}\, \mathrm{d}\mathbf{A} \cdot \Delta \boldsymbol{W}_{\underline{1}}^{(1)} \cdot \delta\mathbf{u} + \int_{(B)} \left(\Delta \boldsymbol{S}_{\underline{1}}^{(1)} \cdot\cdot\, \delta \boldsymbol{E}_{\underline{1}}^{(1)} + \Delta \boldsymbol{S}_{\underline{1}}^{(2)} \cdot\cdot\, \delta \boldsymbol{E}_{\underline{1}}^{(0)} + \Delta \boldsymbol{S}_{\underline{1}}^{(2)} \cdot\cdot\, \delta \boldsymbol{E}_{\underline{1}}^{(1)}\right) \mathrm{d}V \\ &= - \int_{(B)} \boldsymbol{S}_{\underline{1}} \cdot\cdot\, \delta \boldsymbol{E}_{\underline{1}}^{(0)}\, \mathrm{d}V + p \int_{(A_t)} \tilde{p}_{\mathrm{o}}\, \mathrm{d}\mathbf{A} \cdot \boldsymbol{W}_{\underline{1}} \cdot \delta\mathbf{u}\,. \end{aligned} \tag{17}$$

2.3. The load correction stiffness matrix

The finite element discretization of (17) results in a nonlinear system of algebraic equations:

$$\begin{aligned} &\left(\mathbf{K}_{\underline{1}ij}^{L} + \mathbf{K}_{\underline{1}ij}^{G}\right) \Delta\mathbf{t}_{\underline{1}j} - p\,\mathbf{K}_{\underline{1}ij}^{LC}\, \Delta\mathbf{t}_{\underline{1}j} - p\,\mathbf{L}_{\underline{1}ijk}\, \Delta\mathbf{t}_{\underline{1}j}\, \Delta\mathbf{t}_{\underline{1}k} \\ &\quad + \left(\mathbf{G}_{\underline{1}ijk} + \mathbf{C}_{\underline{1}ikj} + \mathbf{H}_{\underline{1}iljk}\, \Delta\mathbf{t}_{\underline{1}l}\right) \Delta\mathbf{t}_{\underline{1}k}\, \Delta\mathbf{t}_{\underline{1}j} = -\mathbf{f}_{\underline{1}i}^{S} + p\,\mathbf{g}_{\underline{1}i}\,, \end{aligned} \tag{18}$$

where $\Delta\mathbf{t}_{\underline{1}j}$ is the vector of the generalized nodal point displacement increments, $\mathbf{K}_{\underline{1}ij}^{L}$ is the linear stiffness matrix, $\mathbf{K}_{\underline{1}ij}^{G}$ is the geometric stiffness matrix, $\mathbf{K}_{\underline{1}ij}^{L} + \mathbf{K}_{\underline{1}ij}^{G} = \mathbf{K}_{\underline{1}ij}^{T}$ is the tangent stiffness matrix, $p\,\mathbf{K}_{\underline{1}ij}^{LC}$ is the load correction stiffness matrix, $-\mathbf{f}_{\underline{1}i}^{S}$ is the vector of nodal point forces equivalent to the element stresses, $p\,\mathbf{g}_{\underline{1}i}$ is the vector of the externally applied nodal point loads, $-\mathbf{f}_{\underline{1}i}^{S} + p\,\mathbf{g}_{\underline{1}i}$ is the vector of the unbalanced nodal point loads in the configuration $(B_{\underline{1}}')$, the subscripts i, j, k, l take the value $1, 2, \ldots, N$, where N is the number of degree of freedom.

The stiffness matrices $\mathbf{K}_{\underline{1}ij}^{L}$, $\mathbf{K}_{\underline{1}ij}^{G}$ are symmetric, consequently $\mathbf{K}_{\underline{1}ij}^{T}$ is also symmetric. The matrix $\mathbf{K}_{\underline{1}ij}^{LC}$ can be either symmetric or non-symmetric depending on whether the load is conservative (that is has a potential) or not conservative (that is has no potential). The terms

$$-p\,\mathbf{K}_{\underline{1}ij}^{LC}\, \Delta\mathbf{t}_{\underline{1}j} - p\,\mathbf{L}_{\underline{1}ijk}\, \Delta\mathbf{t}_{\underline{1}j}\, \Delta\mathbf{t}_{\underline{1}k} \tag{19}$$

in (18) are due to the increment of the surface element vector.

Introducing the notations

$$\begin{aligned}\Delta\mathbf{X}_{\underline{1}i} &= -\mathbf{L}_{\underline{1}ijk}\,\Delta\mathbf{t}_{\underline{1}j}\Delta\mathbf{t}_{\underline{1}k}\\ \Delta\mathbf{Y}_{\underline{1}i} &= \left(\mathbf{G}_{\underline{1}ijk}+\mathbf{C}_{\underline{1}ikj}+\mathbf{H}_{\underline{1}iljk}\Delta\mathbf{t}_{\underline{1}l}\right)\Delta\mathbf{t}_{\underline{1}k}\Delta\mathbf{t}_{\underline{1}j}\end{aligned} \tag{20}$$

the equation (18) can be written as

$$\left(\mathbf{K}^{L}_{\underline{1}ij}+\mathbf{K}^{G}_{\underline{1}ij}\right)\Delta\mathbf{t}_{\underline{1}j}-p\,\mathbf{K}^{LC}_{\underline{1}ij}\,\Delta t_{\underline{1}j}+p\,\Delta\mathbf{X}_{\underline{1}i}+\Delta\mathbf{Y}_{\underline{1}i}=-\,\mathbf{f}^{S}_{\underline{1}i}+p\,\mathbf{g}_{\underline{1}i}\,. \tag{21}$$

2.4. Newton–Raphson iteration method

The nonlinear system of equations (18) or (21) is solved numerically by the Newton–Raphson method. In the first step of the iteration the following linear system of equations is solved

$$\underline{\left(\mathbf{K}^{L}_{\underline{1}ij}+\mathbf{K}^{G}_{\underline{1}ij}\right)\Delta\mathbf{t}_{\underline{1}j}}-\underline{p\,\mathbf{K}^{LC}_{\underline{1}ij}\,\Delta t_{\underline{1}j}}=\underline{-\mathbf{f}^{S}_{\underline{1}i}}+\underline{p\,\mathbf{g}_{\underline{1}i}}\,. \tag{22}$$

Considering equations (22) there are two cases as it is indicated by the underlining:

I. the terms underlined with continuous lines involve the increments of the surface element vectors, i.e., the load correction stiffness matrix,

II. the terms underlined with dashed parallel lines do not involve the load correction stiffness matrix $p\mathbf{K}^{LC}_{\underline{1}ij}$.

After the first iteration step the nodal point displacement vector of the second intermediate configuration $\left(B'_{\underline{2}}\right)$ is of the form

$$\mathbf{t}_{\underline{2}j}=\mathbf{t}_{\underline{1}j}+\Delta\mathbf{t}_{\underline{1}j}\,. \tag{23}$$

In the second step of iteration the equation system linearized in $\Delta t_{\underline{2}j}$ assumes the form

$$\underline{\left(\mathbf{K}^{L}_{\underline{2}ij}+\mathbf{K}^{G}_{\underline{2}ij}\right)\Delta t_{\underline{2}j}}-p\,\mathbf{K}^{LC}_{\underline{2}ij}\,\Delta t_{\underline{2}j}=-\mathbf{f}^{S}_{\underline{2}i}+p\,\mathbf{g}_{\underline{2}i}=\underline{-\left(p\,\Delta\mathbf{X}_{\underline{1}i}+\Delta\mathbf{Y}_{\underline{1}i}\right)}-\left(-p\,\mathbf{K}^{LC}_{\underline{1}ij}\,\Delta\mathbf{t}_{\underline{1}j}\right) \tag{24}$$

where the underlining has the same meaning as above.

Comparing (22) to (24) in case II, one can see that the load correction stiffness matrix which is disregarded in the first step of the iteration appears in the second step on the r.h.s. of equation (24). Therefore, the two iteration methods are similar concerning the essence of the physical contents, but the case I has proved to be numerically more efficient than the case II. In our numerical experiments the number of iterations is smaller at least with one magnitude for the case I if the prescribed tolerance is the same for both cases.

We can see the correctness of (24), e.g., in the case I, if we take into consideration that the unbalanced nodal point load vector $-\mathbf{f}^{S}_{\underline{2}i}+p\,\mathbf{g}_{\underline{2}i}$ associated with the configuration $(B'_{\underline{2}})$ is originated from the formula

$$\begin{aligned}&-\int_{(B)}\boldsymbol{S}_{\underline{2}}\cdot\cdot\,\delta\boldsymbol{E}^{(0)}_{\underline{2}}\,\mathrm{d}V+p\int_{(\bar{A}_t)}\tilde{p}_{\circ}\,\mathrm{d}\mathbf{A}\cdot\boldsymbol{W}_{\underline{2}}\cdot\delta\mathbf{u}\\ &\quad=-\int_{(B)}\left(\boldsymbol{S}_{\underline{1}}+\Delta\boldsymbol{S}^{(1)}_{\underline{1}}+\Delta\boldsymbol{S}^{(2)}_{\underline{1}}\right)\cdot\cdot\left(\delta\boldsymbol{E}^{(0)}_{\underline{1}}+\delta\boldsymbol{E}^{(1)}_{\underline{1}}\right)\mathrm{d}V\\ &\quad\quad+p\int_{(\bar{A}_t)}\tilde{p}_{\circ}\,\mathrm{d}\mathbf{A}\cdot\left(\boldsymbol{W}_{\underline{1}}+\Delta\boldsymbol{W}^{(1)}_{\underline{1}}+\Delta\boldsymbol{W}^{(2)}_{\underline{1}}\right)\cdot\delta\mathbf{u}\,.\end{aligned}$$

With regard to the fact that in the first step of the iteration equation (22) is of the form

$$-\int_{(B)}\left(\boldsymbol{S}_{\underline{1}}\cdot\cdot\,\delta\boldsymbol{E}_{\underline{1}}^{(1)}-\Delta\boldsymbol{S}_{\underline{1}}\cdot\cdot\,\delta\boldsymbol{E}_{\underline{1}}^{(0)}\right)\mathrm{d}V+p\int_{(\bar{A}_t)}\tilde{p}_{\circ}\,\mathrm{d}\mathbf{A}\cdot\Delta\boldsymbol{W}_{\underline{1}}^{(1)}\cdot\delta\mathbf{u}$$
$$-\int_{(B)}\boldsymbol{S}_{\underline{1}}\cdot\cdot\,\delta\boldsymbol{E}_{\underline{1}}^{(0)}\,\mathrm{d}V+p\int_{(\bar{A}_t)}\tilde{p}_{\circ}\,\mathrm{d}\mathbf{A}\cdot\boldsymbol{W}_{\underline{1}}\cdot\delta\mathbf{u}=0,$$

we find for the unbalanced load vector $-\mathbf{f}_{\underline{2}i}^{S}+p\,\mathbf{g}_{\underline{2}i}$ of the configuration $(B_{\underline{2}}')$ — see the right hand side of (24) — that

$$-\int_{(B)}\boldsymbol{S}_{\underline{2}}\cdot\cdot\,\delta\boldsymbol{E}_{\underline{2}}^{(0)}\,\mathrm{d}V+p\int_{(\bar{A}_t)}\tilde{p}_{\circ}\,\mathrm{d}\mathbf{A}\cdot\boldsymbol{W}_{\underline{2}}\cdot\delta\mathbf{u}$$
$$=-\int_{(B)}\left(\Delta\boldsymbol{S}_{\underline{1}}^{(1)}\cdot\cdot\,\delta\boldsymbol{E}_{\underline{1}}^{(1)}+\Delta\boldsymbol{S}_{\underline{1}}^{(2)}\cdot\cdot\,\delta\boldsymbol{E}_{\underline{1}}^{(0)}+\Delta\boldsymbol{S}_{\underline{1}}^{(2)}\cdot\cdot\,\delta\boldsymbol{E}_{\underline{1}}^{(1)}\right)\mathrm{d}V$$
$$+p\int_{(\bar{A}_t)}\tilde{p}_{\circ}\,\mathrm{d}\mathbf{A}\cdot\Delta\boldsymbol{W}_{\underline{1}}^{(2)}\cdot\delta\mathbf{u}.$$

2.5. The end of iteration

Let us write the formulae for the n-th iteration step and for both cases:

$$\underline{\left(\mathbf{K}_{\underline{n}ij}^{L}+\mathbf{K}_{\underline{n}ij}^{G}\right)\Delta\mathbf{t}_{\underline{n}j}}\;-p\,\mathbf{K}_{\underline{n}ij}^{LC}\,\Delta\mathbf{t}_{\underline{n}j}=-\mathbf{f}_{\underline{n}i}^{S}+p\mathbf{g}_{\underline{n}i}$$
$$=\underline{-\left(p\,\Delta\mathbf{X}_{\underline{n-1}i}+\Delta\mathbf{Y}_{\underline{n-1}i}\right)}-\left(-p\,\mathbf{K}_{\underline{n-1}ij}^{LC}\,\Delta\mathbf{t}_{\underline{n-1}j}\right).\qquad(25)$$

Then

$$-\mathbf{f}_{\underline{n+1}i}^{S}+p\,\mathbf{g}_{n+1i}=\underline{-\left(p\,\Delta\mathbf{X}_{\underline{n}i}+\Delta\mathbf{Y}_{\underline{n}i}\right)}-\left(-p\,\mathbf{K}_{\underline{n}ij}^{LC}\,\Delta\mathbf{t}_{\underline{n-1}j}\right)\approx 0_i\qquad(26)$$

and

$$\underline{\left(\mathbf{K}_{\underline{n+1}ij}^{L}+\mathbf{K}_{\underline{n+1}ij}^{G}\right)\Delta\mathbf{t}_{\underline{n+1}j}}\;-p\,\mathbf{K}_{\underline{n+1}ij}^{LC}\,\Delta\mathbf{t}_{\underline{n+1}j}\approx 0_i\qquad(27)$$

if n is large enough.

2.6. Equilibrium paths

Using the incremental form of the principle of virtual displacement, we can find the present equilibrium configuration $(\bar{B})$, if it exists, for any load parameter p. Thus, we can compute points of the equilibrium paths.

There exist two equilibrium paths of special importance. The first is the fundamental path emerging from the reference configuration, the second is the bifurcation path emerging from an appropriately chosen otherwise arbitrary initial configuration $(B_{\underline{1}}')$. The bifurcation point on the fundamental equilibrium path is regarded to be the critical load parameter p_{cr}. It is undeniable that this approach to determine the critical load requires some intuition and cannot be used in general. In what follows we turn our attention to bifurcations on the fundamental equilibrium path.

2.7. Critical load

On the basis of equation (27) we can formulate the following nonlinear eigenvalue problem

$$\mathbf{K}_{\underline{n+1}ij}(p)\,\Delta\mathbf{t}_{\underline{n+1}j} = \underbrace{\left[\mathbf{K}^{L}_{\underline{n+1}ij} + \mathbf{K}^{G}_{\underline{n+1}ij} - p\,\mathbf{K}^{LC}_{\underline{n+1}ij}\right]}_{=====}\Delta\mathbf{t}_{\underline{n+1}j} = 0_i \tag{28}$$

where the stiffness matrices are functions of the load parameter p.

Equation (28) can has a nontrivial solution for $\Delta\mathbf{t}_{\underline{n+1}j}$ if the matrix $\mathbf{K}_{\underline{n+1}ij}$ is singular. The smallest value of the load parameter, p for which the matrix $\mathbf{K}_{\underline{n+1}ij}$ is singular, is denoted by p_{cr}.

For the numerical determination of the smallest eigenvalue we have two mechanical approaches:

A. Using the path following method the first bifurcation point is determined by the help of equilibrium paths. In this way it is also possible to investigate the postcritical equilibrium configurations.

B. Following the fundamental path we determine the value of the load for which the determinant of the total stiffness matrix $\mathbf{K}_{\underline{s}ij}$ vanishes. This procedure cannot be applied for investigating postcritical equilibrium configurations.

It should be mentioned that, due to the nonlinearity of the problem, both methods are based on the incremental form of the principle of virtual displacement and the accuracy of the critical load can be determined only within a prescribed tolerance independently of the methods chosen.

3. Numerical experiments

3.1. Elastic ring with follower loads

Consider a circular ring of rectangular cross-section loaded by inward radial pressure $\tilde{p}$. Knowing that the first buckling mode is symmetric it is enough to investigate a quarter of the ring for which symmetric boundary conditions are imposed on the edges that lie on the axes of symmetry of the deformation (see Fig. 2).

The ring is characterized by the mean radius $R_o = 10\ in$; thickness $t = 1.0$ in; width $b = 1.0$ in; modulus of elasticity $E = 3.0 \times 10^7$ lbf/in^2, Poisson ratio $\upsilon = 0$ and $\tilde{p}_o = -1$ lbf/in^2.

The goal is to determine the critical value p_{cr} of the load factor with the method A of the Section 2.7. (Remainder: the critical load is $\tilde{p}_{cr} = p_{cr}\,\tilde{p}_o$; for our case $\tilde{p}_{cr} = -p_{cr}$ lbf/in^2).

The problem was discussed already in the XIX century by M. Levy [13] and later by S.P. Timoshenko and J.M. Gere [22]. The assumptions used in the classical theory of elastic beams were applied

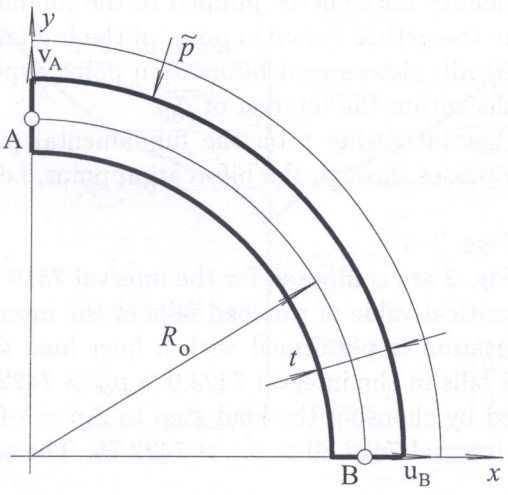

Fig. 2. Elastic ring

and the equations of equilibrium were written for the deformed configuration. The predicted critical load is

$$\tilde{p}_{crL} = -3\frac{EI}{b\,R_o^3}\,; \qquad I = \frac{bt^3}{12}\,, \tag{29}$$

where I is the moment of inertia. For our data (29) yields $\tilde{p}_{crL} = -7500$ lbf/in^2, and $p_{crL} = 7500$.

The buckling problem of the circular ring has been discussed recently by B. Szabó and Gy. Királyfalvi [17]. Their numerical results are in good agreement with those presented in this paper for the same problem.

Assuming one-dimensional model, extensible centre line and for certain conservative loads Gy. Szeidl [18] also investigated the buckling problem of circular arches.

In the present paper hexahedral elements with uniform p-extension ($p = 5$) are used for the finite element model. The number of elements is 10. Convergence is achieved if

$$\sqrt{\frac{\left(\Delta t_{\underline{sj}}\right)^T \Delta t_{\underline{sj}}}{\left(t_{\underline{sj}}\right)^T t_{\underline{sj}}}} \leq \text{tol} \tag{30}$$

where tol $= 10^{-5}$.

Let the radial displacements at the points A and B of the centerline be denoted by v_A and u_B, respectively (see Fig. 2).

3.2. Fundamental and bifurcation paths

We have determined the following equilibrium paths: the load factor p versus the displacement v_A and the load factor p versus the displacement u_B. On the fundamental path the curves p versus v_A and p versus u_B coincide, however, on the bifurcation path they are different.

Two series of computations have been performed with the path following method. In the first series, the initial configuration $(B_{\underline{1}}')$ is the same as the reference configuration (B). The initial value of the load factor p is smaller than p_{crL} and it is increased in the subsequent load steps. In this way we can locate the section of the fundamental equilibrium path which we are interested in.

In the second series, the initial value of the load factor p is greater than p_{crL} and the iteration is started from an appropriately chosen kinematically admissible initial configuration $(B_{\underline{1}}')$. Then the value of p is decreased in the subsequent load steps. In this way two different bifurcation equilibrium paths are determined. The bifurcation equilibrium paths of points A and B are getting close to the bifurcation point and at its vicinity both curves jumped to the fundamental path.

The bifurcation point is the theoretical common point of the fundamental and bifurcation paths.

The accuracy of the numerically determined bifurcation point depends on the value of the load step Δp as the exact value falls within the interval of Δp.

It is worthy of mention that increasing p on the fundamental path and decreasing p on the bifurcation path the iteration passes through the bifurcation point, i.e., abnormal termination does not occur.

The results are shown in Figs. 3–5.

The equilibrium paths in Fig. 3 are computed for the interval $7510 \geq p \geq 7410$ applying equidistant $\Delta p = -5$ steps and the critical value of the load falls in the interval of $7425 > p_{cr} > 7420$.

In this interval the computation is performed with a finer load step $\Delta p = -0.5$ as shown in Fig. 4, where the critical load falls in the interval $7423.0 > p_{cr} > 7422.5$.

Higher accuracy is achieved by choosing the load step to $\Delta p = -0.05$ (see Fig. 5). The critical value of the load falls in the interval $7422.80 > p_{cr} > 7422.75$. The estimated value of the critical load

$$p_{cr} = 7422.79, \qquad \left(\tilde{p}_{cr} = -7422.79 \text{ lbf/in}^2\right),$$

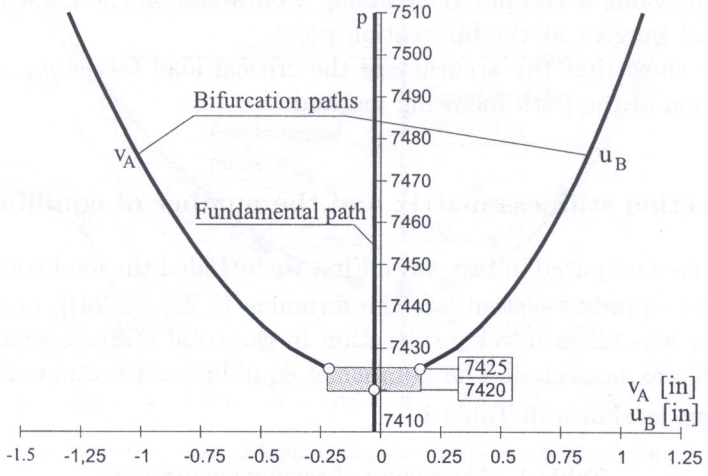

Fig. 3. Circular ring. Equlibrium paths

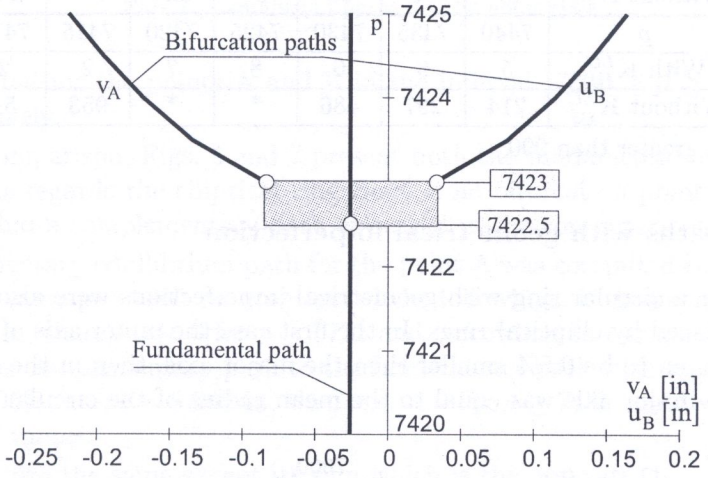

Fig. 4. Circular ring. Equlibrium paths

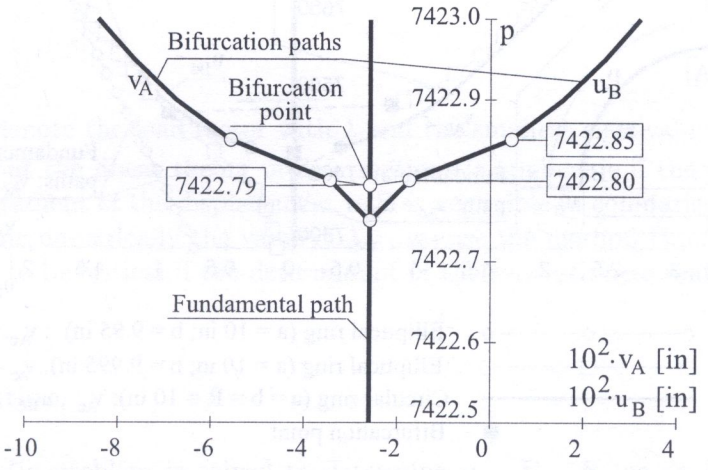

Fig. 5. Circular ring. Equlibrium paths

is shown in Fig. 5. This value is computed by fitting a parabola on the known values in such a way that it has a horizontal tangent at the bifurcation point.

The figures clearly show that the accuracy of the critical load factor p_{cr} can be increased with the repeated application of the path following method.

3.3. The load correction stiffness matrix and the number of equilibrium iterations

The points of Fig. 3 were computed in two ways. First we included the load correction matrix $p\mathbf{K}^{LC}_{\underline{s}ij}$, $\underline{s} = \underline{1}, \underline{2}, \ldots, \underline{n}$ into the equation system [see the formulae (2.22), (2.24)], i.e. the increment of the surface element vector was taken into consideration in the total stiffness matrix. Then the matrix $p\mathbf{K}^{LC}_{\underline{s}ij}$, $\underline{s} = \underline{1}, \underline{2}, \ldots, \underline{n}$ was neglected. The number of equilibrium iterations for the same tolerance $tol = 10^{-5}$ are different as shown in Table 1.

Table 1. The number of equilibrium iterations

p	7510	7500	7490	7480	7470	7460	7450
With $\mathbf{K}^{LC}_{\underline{s}ij}$	13	4	4	4	4	4	5
Without $\mathbf{K}^{LC}_{\underline{s}ij}$	87	50	58	67	80	101	138
p	7440	7435	7430	7425	7420	7415	7410
With $\mathbf{K}^{LC}_{\underline{s}ij}$	5	6	6	8	7	2	2
Without $\mathbf{K}^{LC}_{\underline{s}ij}$	214	297	486	*	*	953	51

* – greater than 990

3.4. Equilibrium paths with geometrical imperfection

Equilibrium paths for a circular ring with geometrical imperfections were also determined, i.e., the circular ring was replaced by elliptical rings. In the first case the minor axis of the centre line of the elliptical ring was chosen to be 0.5% smaller then the major axis, then in the second case the value was 0.05%, while the major axis was equal to the mean radius of the circular ring in both cases.

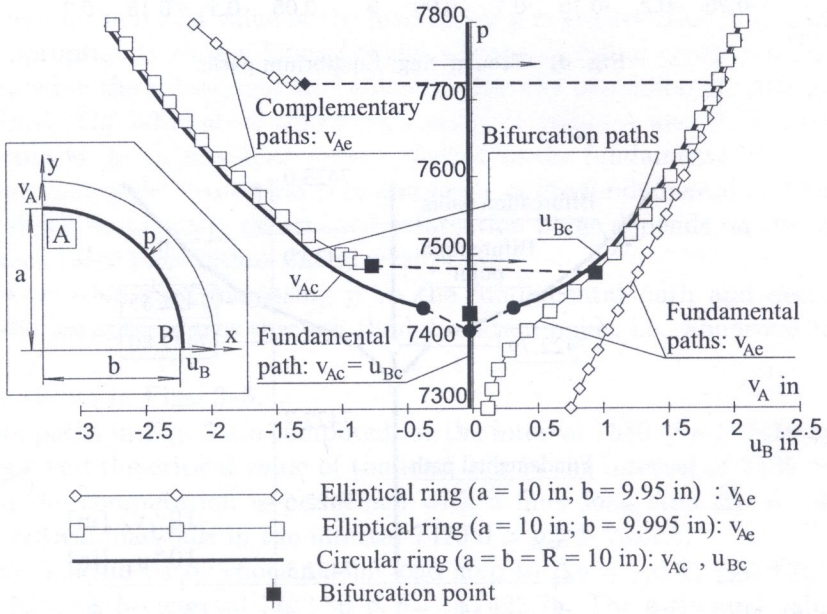

Fig. 6. Equlibrium paths for the point A

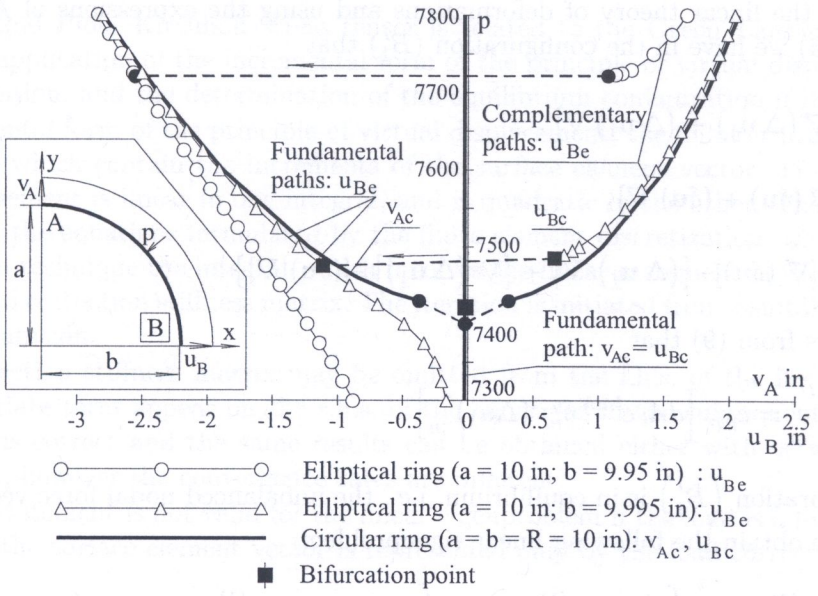

Fig. 7. Equlibrium paths for the point B

The results computed for the points A and B in the interval $7800 \geq p \geq 7300$ are shown in Figs. 6 and 7, respectively.

For the sake of a comparison, Figs. 6 and 7 present both the fundamental and bifurcation paths of the circular ring. As regards the elliptical ring there is no bifurcation point on the fundamental path. On the other hand a complementary path appeared in the computations.

When the complementary equilibrium path for the point A was computed by decreasing the load factor from the initial value p = 7800 we experienced the followings. If the geometrical imperfection is 0.5%, i.e., $b = 9.95$ in, then $v_{Ae} < 0$ for $p \geq 7722$ and, according to our computations, there is a snap-through from this complementary path to the fundamental path with $v_{Ae} > 0$ for $p \leq 7721$. If the imperfection is 0.05%, i.e., $b = 9.995$ in, then $v_{Ae} < 0$ for $p \geq 7485$, and $v_{Ae} > 0$ for $p \leq 7475$ are the corresponding values.

The results for u_{Be} are the same except its sign which is the opposite.

4. Linear eigenvalue problems

4.1. Assumptions

In this section let us denote the load factor with λ and the smallest eigenvalue with λ_{cr} .

We shall assume that the linear theory of deformations is applicable if the load factor $\lambda \leq \lambda_{cr}$. This means that the gradient of the displacement $u_{\underline{1}}\nabla$ is negligible in comparison to the unit tensor $\boldsymbol{I}$. In order to determine numerically the value of λ_{cr} , we use the method B. of Section 2.7, i.e., we regard the load factor to be critical if the determinant of the total stiffness matrix changes its sign.

4.2. The basic equation

In the first step a static problem is solved to determine $\mathbf{u}_{\underline{0}}$, $\boldsymbol{E}_{\underline{0}}$, $\boldsymbol{S}_{\underline{0}}$ as an equilibrium configuration $(B_{\underline{0}})$ for the load $\tilde{p}_{\underline{0}} = -1\,\mathrm{lbf/in^2}$, then the load $\lambda\tilde{p}_{\underline{0}}$ corresponds to the first intermediate configuration $(B'_{\underline{1}})$. In this case, $(B'_{\underline{1}})$ is an equilibrium configuration and $\boldsymbol{S}_{\underline{1}} = \lambda\,\boldsymbol{S}_{\underline{0}}$.

According to the linear theory of deformations and using the expressions of Appendix (A.2a), (A.4a) and (A.5a) we have in the configuration $(B'_{\underline{1}})$ that

$$\Delta \boldsymbol{E}^{(1)}_{\underline{1}} = \frac{1}{2}\left[\nabla\left(\Delta \mathbf{u}_{\underline{1}}\right) + \left(\Delta \mathbf{u}_{\underline{1}}\right)\nabla\right], \tag{31}$$

$$\delta \boldsymbol{E}^{(0)}_{\underline{1}} = \frac{1}{2}\left[\nabla\left(\delta\mathbf{u}\right) + \left(\delta\mathbf{u}\right)\nabla\right], \tag{32}$$

$$\delta \boldsymbol{E}^{(1)}_{\underline{1}} = \frac{1}{2}\left\{\left[\nabla\left(\delta\mathbf{u}\right)\right]\cdot\left[\left(\Delta \mathbf{u}_{\underline{1}}\right)\nabla\right] + \left[\nabla\left(\Delta \mathbf{u}_{\underline{1}}\right)\right]\cdot\left[\left(\delta\mathbf{u}\right)\nabla\right]\right\}. \tag{33}$$

Further it follows from (9) that

$$dA_l \left(\Delta W^{(1)}_{\underline{1}}\right)^l_{\ p} = e_{pqr}\left[dA_l\, e^{lmn}\,\delta^q_m\,\left(\Delta u_{\underline{1}}\right)^r_{\ ;n}\right]. \tag{34}$$

Since the configuration $\left(B'_{\underline{1}}\right)$ is in equilibrium, i.e., the unbalanced nodal force vector is zero, from (17) and (22) we obtain the following linear eigenproblem:

$$\int\limits_{(B)} \triangle \boldsymbol{S}^{(1)}_1 \cdot\cdot \delta \boldsymbol{E}^{(0)}_1 \mathrm{d}V + \int\limits_{(B)} \mathbf{S}_{\underline{\underline{\circ}}} \cdot\cdot \delta \boldsymbol{E}^{(1)}_1 \mathrm{d}V - \lambda \int\limits_{(A_t)} \tilde{p}_{\underline{\underline{\circ}}}\, \mathrm{d}\mathbf{A}\cdot \triangle \boldsymbol{W}^{(1)}_{\underline{1}} \cdot \delta\mathbf{u} = 0\,, \tag{35}$$

$$\mathbf{K}^{L}_{\underline{1}ij}\,\Delta t_{\underline{1}j} + \lambda\,\mathbf{K}^{G}_{\underline{\underline{\circ}}ij}\,\Delta t_{\underline{1}j} - \lambda\,\mathbf{K}^{LC}_{\underline{1}ij}\,\Delta t_{\underline{1}j} = 0_i \tag{36}$$

As regards the integrals of formula (35) and the matrices $\mathbf{K}^{L}_{\underline{1}ij}$, $\mathbf{K}^{G}_{\underline{\underline{\circ}}ij}$ and $\mathbf{K}^{LC}_{\underline{1}ij}$ in (36) they do not depend on the displacement field of the configuration $(B'_{\underline{1}})$ therefore the underlined index $\underline{1}$ can be omitted.

Considering (36), and of course, (35) we can read an important statement:

- the formula (36) can be applied only to follower loads (both for a non-conservative load and for a conservative one), if the load correction matrix $\mathbf{K}^{LC}_{\underline{1}ij}$ is included, otherwise (36) is applicable only to those loads which maintain their direction.

Solving the example of Section 3.1 with the determinant search method we obtain for the smallest eigenvalue of the linear eigenproblem for non-conservative follower loads that

$$\lambda_{cr} = 7424.9, \qquad \tilde{p}_{cr} = -\,7424.9\ \mathrm{lbf/in^2}.$$

It is worthy of recalling the results

$$\lambda_{cr} = 7422.79 \quad \text{and} \quad \tilde{p}_{cr} = -\,7422.79\ \mathrm{lbf/in^2}$$

obtained by solving the nonlinear problem by the path-following method – see Section 3.3 for further details.

5. Concluding remarks

5.1. Effect of the increment of the surface element vector in the cases of follower loads

The object of this paper is the investigation of elastic bodies loaded by nonconservative follower loads, which are normal to the instantaneous surface of the body. The main features of the investigations are: static method, three-dimensional and geometrically nonlinear model, total Lagrangian

description, the 2nd Piola–Kirchhoff stress tensor is related to the Green–Lagrange strain tensor by Hooke's law, application of the incremental form of the principle of virtual displacements, finite element discretization, and the determination of the equilibrium configuration if it exists.

In the incremental form of the principle of virtual displacement, the follower loads are present in the two integrals which contain the increments of the surface element vector. The gradient of the displacement increment is linear in one integral, and is quadratic in the other. Therefore, there are also two terms in the equations formulated by the finite element discretization. Using the Newton–Raphson iteration technique the integral, which involves the linear increment of the surface element vector, gives a load correction stiffness matrix. The iteration is initiated from a suitable kinematically admissible configuration.

The load correction stiffness matrix may be omitted from the l.h.s. of the iteration equations, since the appropriate term appear on the r.h.s. of the equations in the subsequent iteration steps. In principle this is correct and the same results can be obtained either with or without the load correction matrix, however the convergence rates are different.

The previous statement is not valid for the linear eigenproblem if the load is a follower one, since the increment of the surface element vector is represented only by the load correction matrix.

5.2. Numerical determination of critical loads

Critical loads for the nonlinear eigenvalue problems are computed by applying two techniques each resting on the finite element method. The first is the path following method, the second is the determinant search algorithm.

5.3. Numerical results of a circular ring

The examples concern a circular ring of rectangular cross-section loaded with uniform inward pressure.

The number of iteration is greater by one magnitude when the load correction stiffness matrix is omitted from the l.h.s. of the equations. The critical value of the load factor is the common point of the fundamental equilibrium path and the bifurcation paths.

When the circular ring is replaced by elliptical ring as a model for a small geometrical imperfection, no bifurcation point appears on the fundamental path, however the appearance of a complementary path is demonstrated by the computations.

Appendix

The quantities in (11), (12) and (14) are detailed with invariant and in index notation in the following:

$$\underline{\boldsymbol{E}}_1 = \frac{1}{2}\left[\nabla \underline{\mathbf{u}}_1 + \underline{\mathbf{u}}_1 \nabla + (\nabla \underline{\mathbf{u}}_1) \cdot (\underline{\mathbf{u}}_1 \nabla)\right] \tag{A.1a}$$

$$(\underline{E}_1)_{kl} = \frac{1}{2}\left[(\underline{u}_1)_{k;l} + (\underline{u}_1)_{l;k} + (\underline{u}_1)_{m;k}\,(\underline{u}_1)^m_{\ ;l}\right] \tag{A.1b}$$

$$\Delta \underline{\boldsymbol{E}}^{(1)}_1 = \frac{1}{2}\left\{\nabla(\Delta \underline{\mathbf{u}}_1) + (\Delta \underline{\mathbf{u}}_1)\nabla + (\nabla \underline{\mathbf{u}}_1) \cdot [(\Delta \underline{\mathbf{u}}_1)\nabla] + [\nabla(\Delta \underline{\mathbf{u}}_1)] \cdot (\underline{\mathbf{u}}_1 \nabla)\right\} \tag{A.2a}$$

$$\left(\Delta \underline{E}^{(1)}_1\right)_{kl} = \frac{1}{2}\left[(\Delta \underline{u}_1)_{k;l} + (\Delta \underline{u}_1)_{l;k} + (\underline{u}_1)_{m;k}\,(\Delta \underline{u}_1)^m_{\ ;l} + (\Delta \underline{u}_1)_{m;k}\,(\underline{u}_1)^m_{\ ;l}\right] \tag{A.2b}$$

$$\Delta \boldsymbol{E}_{\underline{1}}^{(2)} = \frac{1}{2}\left[\nabla\left(\Delta \mathbf{u}_{\underline{1}}\right)\right] \cdot \left[\left(\Delta \mathbf{u}_{\underline{1}}\right) \nabla\right] \tag{A.3a}$$

$$\left(\Delta E_{\underline{1}}^{(2)}\right)_{kl} = \frac{1}{2}\left(\Delta u_{\underline{1}}\right)_{m;k}\left(\Delta u_{\underline{1}}\right)^{m}_{;l} \tag{A.3b}$$

$$\delta \boldsymbol{E}_{\underline{1}}^{(0)} = \delta\left(\Delta \boldsymbol{E}_{\underline{1}}^{(1)}\right) = \frac{1}{2}\left\{\nabla\left(\delta \mathbf{u}\right) + \left(\delta \mathbf{u}\right)\nabla + \left(\nabla \mathbf{u}_{\underline{1}}\right) \cdot \left[\left(\delta \mathbf{u}\right)\nabla +\right] + \left[\nabla\left(\delta \mathbf{u}\right)\right] \cdot \left(\mathbf{u}_{\underline{1}}\nabla\right)\right\} \tag{A.4a}$$

$$\left(\delta E_{\underline{1}}^{(0)}\right)_{kl} = \left[\delta\left(\Delta E_{\underline{1}}^{(1)}\right)\right]_{kl} = \frac{1}{2}\left[\left(\delta u\right)_{k;l} + \left(\delta u\right)_{l;k} + \left(u_{\underline{1}}\right)_{m;k}\left(\delta u\right)^{m}_{;l} + + \left(\delta u\right)_{m;k}\left(u_{\underline{1}}\right)^{m}_{;l}\right] \tag{A.4b}$$

$$\delta \boldsymbol{E}_{\underline{1}}^{(1)} = \delta\left(\Delta \boldsymbol{E}_{\underline{1}}^{(2)}\right) = \frac{1}{2}\left\{\left[\nabla\left(\delta \mathbf{u}\right)\right] \cdot \left[\left(\Delta \mathbf{u}_{\underline{1}}\right)\nabla\right] + \left[\nabla\left(\Delta \mathbf{u}_{\underline{1}}\right)\right] \cdot \left[\left(\delta \mathbf{u}\right)\nabla\right]\right\} \tag{A.5a}$$

$$\left(\delta E_{\underline{1}}^{(1)}\right) = \left[\delta\left(\Delta E_{\underline{1}}^{(2)}\right)\right]_{kl} = \frac{1}{2}\left[\left(\delta u\right)_{m;k}\left(u_{\underline{1}}\right)^{m}_{;l} + \left(\Delta u_{\underline{1}}\right)_{m;k}\left(\delta u\right)^{m}_{;l}\right] \tag{A.5b}$$

and for example

$$\Delta \boldsymbol{S}_{\underline{1}}^{(1)} = \Delta \boldsymbol{E}_{\underline{1}}^{(1)} \,..^{[4]}\boldsymbol{C}, \qquad \left(\Delta S_{\underline{1}}^{(1)}\right)^{mn} = \left(\Delta E_{\underline{1}}^{(1)}\right)_{kl}{}^{[4]}C^{klmn}. \tag{A.6}$$

Acknowledgements

Authors gratefully express their acknowledgements to Professor Barna Szabó of Washington University in St. Louis, USA for his drawing our attention to the problem of follower loads and for the helpful discussions on the intermediate results.

The support provided by the Hungarian National Research Foundation (OTKA No. T22022/97) is also gratefully acknowledged.

References

[1] J.H. Argyris, K. Straub, Sp. Symeonidis. Nonlinear finite element analysis of elastic systems under nonconservative loading — natural formulation. Part II. Dynamic problems. *Comput. Meths. Appl. Mech. Engng.*, **8**: 241–258, 1981.

[2] J.H. Argyris, K. Straub, Sp. Symeonidis. Static and dynamic stability of nonlinear systems under nonconservative forces — natural approach. *Comput. Meths. Appl. Mech. Engng.*, **32**: 59–83, 1982.

[3] J.H. Argyris, Sp. Symeonidis. Nonlinear finite element analysis of elastic systems under nonconservative loading — natural formulation. Part I. Quasistatic problems. *Comput. Meths. Appl. Mech. Engng.*, **26**: 75–124, 1981.

[4] J.H. Argyris, Sp. Symeonidis. A sequel to: Nonlinear finite element analysis of elastic systems under nonconservative loading — natural formulation. Part I. Quasistatic problems. *Comput. Meths. Appl. Mech. Engng.*, **26**: 377–383, 1981.

[5] V.V. Bolotin. *Nonconservative Problems of the Theory of Elastic Stability.* Pergamon, New York, 1963.

[6] G.A. Cohen. Conservativeness of a normal pressure field acting on a shell. *AIAA J.*, **4**: 1886, 1966.

[7] M.A. Crisfield. *Non-linear Finite Elemente Analysis of Solids and Structures*, volume 2. Wiley, London, 1997.

[8] H.Foegel, H.A. Mang. Zum Einfluss der Verschiebungsabhaengigkeit ungleichförmigen hydrostatischen Druckes auf das Ausbeulen dünner Schalen allgemeiner Form. *Int. J. Num. Meths. Engng.*, **15**: 15–30, 1981.

[9] A.N. Guz. *Fundamentals for Three Dimensional Theory of Stability of Deformable Bodies* (in Russian). Visa Skola, Kiev, 1986.

[10] H.D. Hibbitt. Some follower forces and load stiffness. *Int. J. Num. Meths. Engng.*, **14**: 937–941, 1979.

[11] K. Huseyin. *Nonlinear Theory of Elastic Stability.* Nordhoff, 1975.

[12] W.T. Koiter. General equations of elastic stability for thin shells. In: *Theory of Thin Shell*, 187–230, University of Houston Press, 1967.

[13] M.M. Levy. Mémoir sur un nouveau cas integrable du probleme de l'elastique etc. *Journal de Math. Liouvill*, **S.3**: 5, 1984.

[14] K. Loganathan, S.C. Chang, R.H. Gallagher, J.F. Abel. Finite element representation and pressure stiffness in shell stability analysis. *Int. J. Num. Meths. Engng.*, **14**: 1413–1420, 1979.

[15] H.A. Mang. Symmetricability of pressure stiffness matrices for shells with loaded free edges. *Int. J. Num. Meths. Engng.*, **15**: 15–30, 1981.

[16] K. Schweizerhof. *Nichtlineare Berechnung von Tragwerken unter Verformungsabhaengiger Belastung mit finiten Elementen.* Diss., Stuttgart, Univ., 1982.

[17] B. Szabó, Gy. Királyfalvi. Linear models of buckling and stress-stiffening. *Comput. Meths. Appl. Mech. Engng.*, **171**: 43–59, 1999.

[18] Gy. Szeidl. *Effect of Change in Lenght on the Natural Frequencies and the Stability of Circular Arches* (in Hungarian). Ph. d. thesis, University of Miskolc, Hungary, 1975.

[19] J.M.T. Thompson. *Instabilities and Catastrophes in Sciences and Engineering.* Wiley, London, 1982.

[20] J.M.T. Thompson, G. W. Hunt. *A General Theory of Elastic Stability.* Wiley, London, 1973.

[21] J.M.T. Thompson, G. W. Hunt. *Elastic Instability Phenomena.* Wiley, London, 1984.

[22] S. P. Timoshenko, J. M. Gere. *Theory of Elastic Stability.* McGraw–Hill, New York, 1961.